Bull Volcanol (2012) 74:2187–2203
DOI 10.1007/s00445-012-0655-4

RESEARCH ARTICLE

The recent Plinian explosive activity of Mt. Pelée volcano (Lesser Antilles): The P1 AD 1300 eruption

Guillaume Carazzo · Steve Tait · Edouard Kaminski · James E. Gardner

Received: 12 November 2011 / Accepted: 6 September 2012 / Published online: 27 September 2012

Abstract Plinian explosive eruptions represent a major volcanic hazard in the Lesser Antilles Arc that must be carefully assessed based on reconstructions of past activity. The present study focusses on a detailed time evolution of the P1 eruption (AD 1300) at Mt Pelée volcano (Martinique). After an initial dome-forming stage, a Plinian phase commenced. The P1 Plinian-style sequence is mostly a pumice fall deposit with an inversely graded base, interbedded with a surge deposit, and overlain by final flow/surge deposit. Field data on deposit dispersal, thickness, and grain-size distribution are used together with physical models to reconstruct the dynamical evolution of this eruption. We find that the mass eruption rate increased from 2×10^7 to 9×10^7 kg s^{-1}, producing a 19–22-km-high Plinian plume, initially stable but which ultimately collapsed to form a ~1.3-km-high fountain. Empirical models of deposit thinning suggest that the minimum volume of pyroclastic deposits is 0.15 km^3, about 25 % that previously estimated. Published data on magmatic water contents in glass inclusions are used together with mass discharge rates to elucidate the mechanisms leading to column collapse. Conditions at the base of the column were close to the plume/fountain transition soon after the Pelean/Plinian-style transition due to the competing effects of increase in both gas content and mass discharge rate. After a short stage of partial collapse, the column underwent a total collapse due to an increasing discharge rate.

Keywords Mt Pelée volcano · Plinian eruption · Tephra dispersal · Column collapse · Eruptive dynamics

Editorial responsibility: T. Thordarson

Electronic supplementary material The online version of this article (doi:10.1007/s00445-012-0655-4) contains supplementary material, which is available to authorized users.

G. Carazzo (✉) · S. Tait · E. Kaminski
Institut de Physique du Globe, Sorbonne Paris Cité, Université Paris Diderot, CNRS UMR 7154 - Dynamique des Fluides Géologiques, 1 rue Jussieu, 75238 Paris Cedex 05, France
e-mail: carazzo@ipgp.fr

S. Tait
e-mail: tait@ipgp.fr

E. Kaminski
e-mail: kaminski@ipgp.fr

J. E. Gardner
Department of Geological Sciences, The University of Texas at Austin, 1 University Station C1100, Austin, TX 78712-0254, USA
e-mail: gardner@mail.utexas.edu

Introduction

Despite its current quiescence, Mt Pelée in Martinique is one of the most active volcanoes of the Lesser Antilles Arc with more than 20 magmatic events over the past 5,000 years (Westercamp and Traineau 1983a) including the May 8, 1902 lateral blast, which destroyed the town of St Pierre and killed more than 28,000 people (Lacroix 1904). This catastrophic (Pelean) event represents only one of the two recurrent types of eruptions at Mt Pelée, and like other stratovolcanoes in the Lesser Antilles, Mt Pelée is capable of producing

powerful explosive (Plinian) eruptions (Roobol and Smith 1980; Westercamp and Traineau 1983a).

The last Plinian eruption at Mt Pelée volcano, named P1, is dated around AD 1300 using ^{14}C by Westercamp and Traineau (1983a). This eruptive event is characterized by a succession of a dome-forming and Plinian activity in a short time interval (Villemant et al. 1996; Villemant and Boudon 1999). During the Plinian phase, the eruption produced an atmospheric ash plume, which ultimately collapsed at ground level producing massive pyroclastic density currents (Westercamp and Traineau 1983a; Bardintzeff et al. 1989; Traineau et al. 1989). Although the Pelean/Plinian style transition has been extensively investigated in previous studies, the time-dependent dynamics of the Plinian phase have not been discussed in detail nor have the mechanisms responsible for the final column collapse been investigated. This paper addresses these issues by reconstructing a detailed time evolution of the eruptive parameters of the P1 eruption based on a new comprehensive field study, and by using physical models to discuss the mechanisms controlling the dynamics of Plinian eruptions.

Mt Pelée volcano

Volcanic activity

Three major phases of volcanic edifice construction in northern Martinique can be distinguished (Westercamp and Traineau 1983a). The first stage, which took place between 400 and 150 ka at the northern edge of the present cone (Mt Conil in Fig. 1), comprises alternations of thick andesitic lava flows and voluminous pyroclastic flow deposits, some well preserved (Tombeau des Caraïbes). The second phase, between 150 and 13.5 ka at Morne Macouba (Fig. 1), consists of a series of alternating pumice falls, pumice flows, block-and-ash

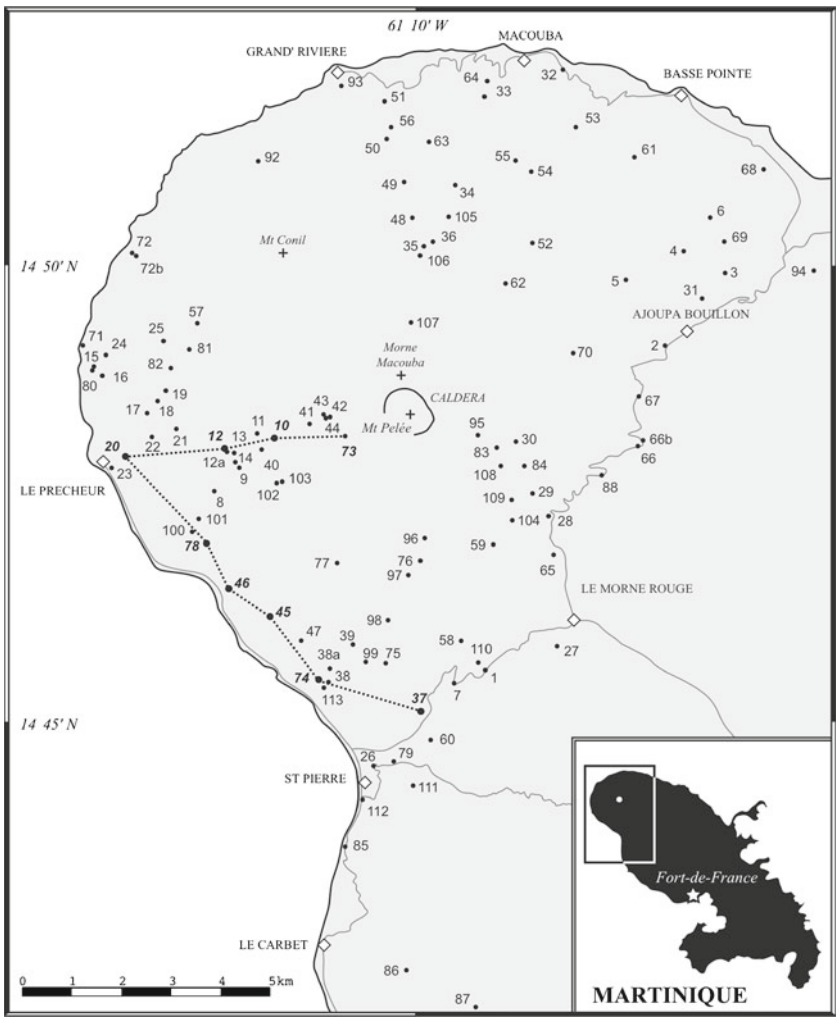

Fig. 1 Map of Martinique (*inset*) showing the locations of Mt Pelée volcano, Morne Macouba, and Mt Conil (*crosses*). The locations of the main towns (*open diamonds*), roads (*solid lines*), and outcrops studied (*solid dots*) are also reported. *Numbers* next to *solid dots* give the number of the sites studied, which are referenced in the paper. *Dotted lines* give the stratigraphic correlation reported in section "Distribution of P1 deposits"

flows, together representing ~1 km^3 of magma emitted during the entire phase (Westercamp and Traineau 1983a, b). The last stage of edifice construction began after 13.5 ka at the present active cone location, characterized by at least ten magmatic events before 5 ka and 24 eruptions in the past 5,000 years (Westercamp and Traineau 1983a).

The period 5000 BP to the present has been documented in several field-based studies (Roobol and Smith 1976, 1980; Traineau 1982; Westercamp and Traineau 1983a, b; Bardintzeff et al. 1989; Bourdier et al. 1989; Traineau et al. 1989), and is characterized by a heterogeneous succession of dome collapse (NPM1, NPM2, NAB2, NMP1, NMP2, 1929), directed blast (NRS1, NRS2, NRS3, NAB1, NRC1, NRC2, NRP1, NRP2, NRP3, 1902), and more voluminous explosive eruptions (P6 to P1), which consisted of either Plinian plumes with subsequent column collapse (P5, P3, P2, and P1) or fountains associated with pyroclastic density currents (P6, P4) (Fig. 2a). The volcanic rocks of Mt Pelée all have similar intermediate bulk composition (andesite to dacite) with high CaO and Al_2O_3 contents, low TiO_2 and K_2O contents, and low MgO/FeO ratios (Dupuy et al. 1985). Petrologic studies and phase equilibrium experiments showed that the transition between Plinian eruptions and dome-forming/directed-blast eruptions is not related to systematic variations in pre-eruptive magmatic water contents (Martel et al. 1998, 2000). The diversity of explosive eruptive styles observed at Mt Pelée volcano has been attributed to differences in interactions of rising magma with hydrothermal fluids, as suggested by analyses of residual H_2O, halogen (Martel et al. 1998; Villemant and Boudon 1998, 1999; Martel et al. 2000), and U-series isotope content (Villemant et al. 1996) in the P1, 1902, and 1929 products. Within this framework, Plinian eruptions are more likely to occur during closed-system degassing in the conduit, whereas open-system degassing results in less powerful dome-forming eruptions.

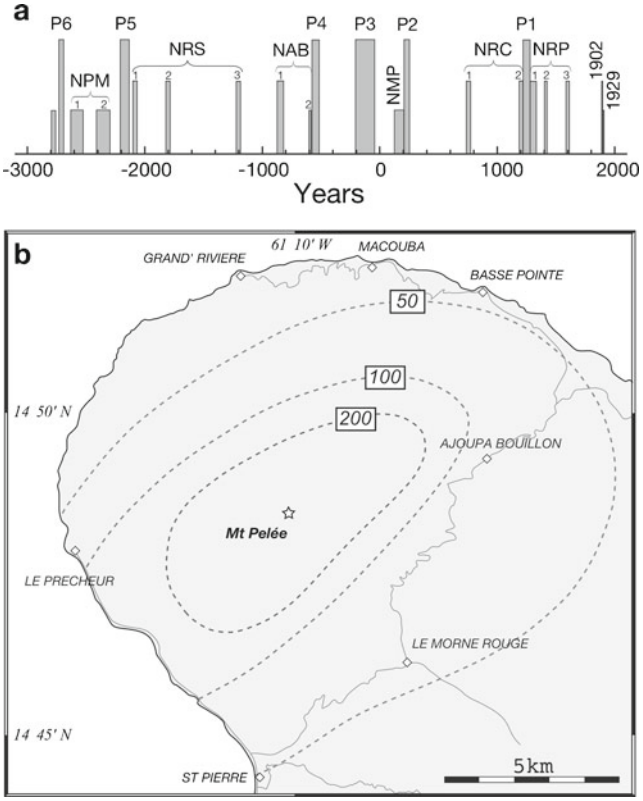

Fig. 2 **a** Eruptive history of Mt Pelée volcano for the past 5,000 years. For each eruption, the width of the *gray bar* corresponds to the uncertainty in eruption age. The height of the *gray bar* indicates the eruption style (*short*, dome collapse; *intermediate*, directed blast; *long*, Plinian). The names of the eruptions are as follows: *NPM*, Nuées ardentes Pointe la Mare; *NRS*, Nuées ardentes Rivière Sèche; *NAB*, Nuées ardentes Ajoupa Bouillon; *NMP*, Nuées ardentes Morne Ponce; *NRC*, Nuées ardentes Rivière Claire; *NRP*, Nuées ardentes Rivière des Pères; *P*, Plinian (modified from Westercamp and Traineau (1983a)). **b** Isopach map (in centimeters) of the Plinian fall deposits of P1 (modified from Traineau et al. (1989)). The dispersal axis reflects the moderate southwesterly antitrade winds blowing between 11- and 21-km altitude

Overview of the most recent Plinian eruption

P1 deposits were first identified by Roobol and Smith (1976, 1980) and mapped by Westercamp and Traineau (1983a). Later, Traineau et al. (1989) and Bardintzeff et al. (1989) provided more detailed descriptions of the deposits and some preliminary estimates of eruptive parameters. The P1 eruption began with brief phreatic activity which produced ash-fall layers. According to Westercamp and Traineau (1983a) and Traineau et al. (1989), this initial stage was followed by the formation of a 21 ± 1-km-high Plinian column. Plinian fall deposits are dispersed along a southwest–northeast axis consistent with moderate antitrade winds blowing between 11- and 21-km altitude (Fig. 2b). The end of the eruption was characterized by column collapse that produced pyroclastic density currents whose deposits are mostly channelized in the Prêcheur and Sèche rivers (Westercamp and Traineau 1983a; Bardintzeff et al. 1989; Traineau et al. 1989).

More recently, Villemant et al. (1996) showed that a violent explosion associated with the destruction of a lava dome took place between the initial phreatic phase and the Plinian activity. The reconstruction of the degassing paths of both Pelean and Plinian regimes using particle densities, H_2O, halogen (Cl, F, Br) (Villemant

and Boudon 1999), U-series isotopes (Villemant et al. 1996), and noble gas content measurements (Ruzié and Moreira 2010) showed that the transition from a dome-forming to a Plinian style during the P1 eruption corresponds to the end of magma interactions with wall-rock and hydrothermal systems. Experimental studies of pre-eruptive conditions and microscopic texture analyses confirm this conclusion (Martel et al. 1998, 2000; Pichavant et al. 2002; Martel and Poussineau 2007) and provide quantitative estimates of pre-eruptive magma storage conditions, including temperature (~1,173 K), pressure (~2 kbar), and water content (~5.5 wt%) (Martel et al. 1998).

Methods

Study of proximal units

The P1 sequence was identified at 53 sites (Fig. 1) over 113 outcrops studied in order to compare our results with those of Traineau et al. (1989) (Fig. 2b). The deposits formed by the Pelean activity have been extensively studied, so the present work focuses on the deposits formed by the Plinian phase. P1 deposits are easily recognizable and can be used to reconstruct the eruption sequence. Where the top of the sequence is missing, P1 deposits can often be recognized by the presence of a thick, dark brown soil at its base. To the west of Mt Pelée's summit, the underlying deposits correspond to the P3 eruption (~2000 BP) characterized clearly by a strong internal layering.

The thickness of each layer of P1 at every site was measured in order to construct isopach maps used to calculate the volume of the deposits and the average column heights. The sizes of the coarsest lithic fragments were measured in many of the fall layers at most sites in order to construct isopleth maps used to constrain the maximum column heights and exit velocities. For this, we excavated a standard area of each layer and measured the major axes of the five largest lithic fragments found.

Grain-size sampling and sieving

We have made grain size analyses of nine samples of the P1 fall deposits with the aim of quantifying the effect of gas entrapment by pumice at fragmentation (Kaminski and Jaupart 1998). For this, samples of single sublayers were carefully collected from the top down of three sections in order to estimate the size distribution for the lapilli fraction of the deposits. The samples were then dried for 24 h in an oven and sieved by hand down to -2ϕ. A binocular microscope was used to discard crystals and lithic fragments in the size range -4 to -2ϕ. Volume calculations for isomass maps for each ϕ interval were then used to infer the grain-size distributions of single sublayers.

Although not a conventional method, cumulative frequency curves were determined following the method of Kaminski and Jaupart (1998). Using 62 grain-size distributions for several Plinian populations, Kaminski and Jaupart (1998) showed that the number of fragments (Δ) in each sieve class ϕ systematically follows closely the equation:

$$\Delta = N_{\mathrm{ref}}\phi^{-D}, \tag{1}$$

where N_{ref} is a normalization constant, and D is the power law exponent. This equation reflects a power law size distribution,

$$N\left(R_p \geq r_p\right) = \lambda r^{-D}, \tag{2}$$

where $N\left(R_p \geq r_p\right)$ is the number of fragments greater than r_p, and λ is a normalization constant. The coefficient D fully characterizes the grain-size distribution and is generally found to be close to 3.

The exact value of D is imposed by the production of fine ash at fragmentation. Where fragmentation is efficient, the production of fine ash is enhanced, D is large (3.3–3.4) and most of the exsolved gas is free. On the other hand, where fragmentation is poorly efficient, D is small (2.9–3.0) and a large amount of exsolved gas is trapped by coarse lapilli pumice. The coefficient D gives the fraction of these two types of fragments and it controls the total amount of gas available. Kaminski and Jaupart (1998) demonstrated that D can be estimated accurately using data at lapilli size only and that it takes gross changes in the sieve data to affect its value. Thus, the lack of fine particles lost out at sea does not affect our estimations of D, and a detailed reconstruction of the total grain-size distribution is not necessary for the purposes of this study.

Calculation of eruptive parameters

The volume of the fall deposits has been obtained by the methods of Pyle (1989) and Legros (2000) based on proximal thinning and from a single isopach, respectively. As we shall see, more sophisticated models could not be used on our dataset. The volume of surge deposits has been calculated using an empirical relationship between the area covered by pyroclastic surges and their volume (Calder et al. 1999).

The maximum column heights associated with the Plinian fall deposits have been estimated from the

distribution of lithic fragments in the field using the method of Carey and Sigurdsson (1989), which is an extension of the model of Carey and Sparks (1986). The average column heights have been calculated using an alternative method based on the change in thinning behavior of deposits along the cross-wind range (Bonadonna et al. 1998). This technique requires modeling of the volcanic column in order to retrieve the mean column height from the position of the break-in slope. The models of Sparks (1986), Woods (1988), and Carazzo et al. (2008a) are used, in turn, for the sake of comparison. The maximum height of the volcanic fountain feeding the eruption during the final column collapse is calculated using the model of Doyle et al. (2010).

Maximum mass discharge rates have been calculated using the classical method of Sparks (1986) with the maximum column heights inferred from the model of Carey and Sigurdsson (1989). Mean mass discharge rates have been calculated using the model of Carazzo et al. (2008a) with mean column heights constrained by the change in thinning behavior of deposits along the cross-wind range. A third method based on the sedimentation model of Bursik et al. (1992) has also been used to calculate mean mass discharge rates. Mass discharge rates for the collapsing phases have been calculated using the model of Bursik and Woods (1996).

A revisit of the P1 deposits

Stratigraphy

A composite stratigraphic column for the P1 deposit is shown in Fig. 3. The sequence starts with a very thin ash-fall unit (BU1) overlain by two thin ash beds (BU2 and BU3). Immediately above these basal units is a thick pumice fall layer (P1A) overlain by a thin ash layer (P1B). The next units consist of another thick pumice fall layer (P1C) and then pyroclastic density current deposits (P1D). The basal layers have already been described and interpreted in previous studies (Traineau et al. 1989; Villemant et al. 1996; Martel et al. 2000). Here, we focus on the description of the pumice fall layer and subsequent units.

Basal units

The first layer in the sequence is a very thin (~1 cm) gray ash bed. It is stratified, unconsolidated, rich in accidental lapilli-size lithic material, and locally contains accretionary lapilli (Traineau et al. 1989), which suggests that this layer results from a short initial phreatic phase (Traineau et al. 1989; Villemant et al. 1996). The lack of erosion or weathering on top of the unit shows that there was no time break between the deposition of

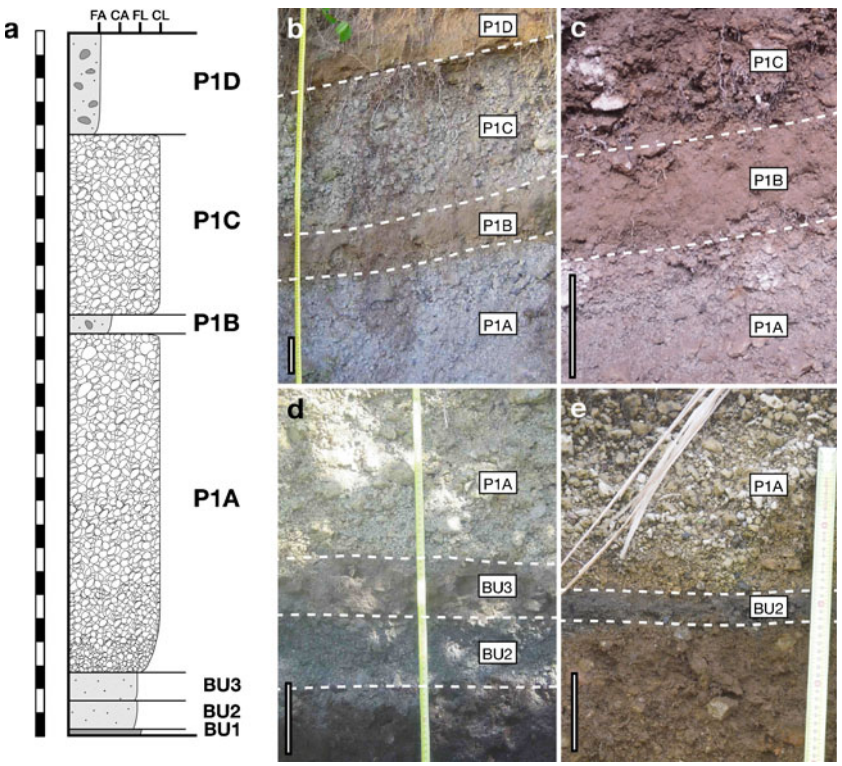

Fig. 3 **a** Composite stratigraphic section showing typical unit thickness and grain size characteristics. **b** Units P1A, P1B, P1C, and P1D at site 10 (2.75 km from the volcano). **c** Units P1A, P1B, and P1C at site 101 (4.75 km). **d** Basal units 2 and 3 (BU2, BU3) and unit P1A at site 74 (5.1 km). **e** Basal unit 2 and unit P1A at site 99 (5.2 km). Boundaries between units are marked by *white dashed lines* in **b–e**. All *scale bars* are 10 cm long

this basal layer and overlying units, which suggests that they were parts of the same event.

Immediately above the basal unit are two thin (< 10 cm) dark-gray ash beds identified by Villemant et al. (1996) and named HVPF1 and HVPF2 by Martel et al. (2000). Both layers are locally cross-bedded and rich in juvenile lapilli-size lithic material, which suggests they resulted from violent explosions associated with the destruction of one or several lava domes (Villemant et al. 1996; Villemant and Boudon 1998, 1999). The duration of this phase of dome construction and destruction is unknown but might have been ~1 or even several years as suggested by the current activity of the Soufriere Hills volcano in Montserrat. The sharp contact between these deposits and the overlying unit suggests, however, that the end of the initial phase that formed the basal units was rapidly followed by the onset of the next eruptive phase (Villemant et al. 1996; Villemant and Boudon 1999).

P1A unit

The main layer of the P1 sequence is a blanket of clast-supported, white pumice lapilli. Unit P1A contains juvenile lithic fragments in an amount that typically increases from 4 wt% at base to 8 wt% at top. At most sites, both pumice and maximum lithic size increase slightly upwards by 25 %. This inverse grading is most pronounced in the lower 1–5 cm of the deposit with pumice sizes increasing from fine to coarse lapilli. The fine-grained base has minor amounts of juvenile lithic material (< 1 wt%) and is the thickest at sites 5–7 km away from the volcano.

In the downwind direction, unit P1A has a maximum measured thickness of 580 cm at 3 km from the crater, steadily thinning to ~160 cm within 5 km of the vent. In the cross-wind direction, unit P1A is 100-cm thick in the most proximal sections, thinning to 40 cm within 5 km of the volcano. The relatively widespread nature of this deposit, its uniformly decreasing thickness with distance from the source, its fabric (inverse grading), framework (clast-supported), and grain type (pumice and juvenile lithic fragments) characteristics indicate that unit P1A is a fall deposit.

P1B unit

P1B is a unit of brown ash-grade material where lithic fragments and crystals are floating in a matrix of dense, angular, glass fragments. All fragments range from fine to coarse ash. Both juvenile and accidental lithic fragments account for less than ~10 wt% combined. At many proximal sites, P1B is finely laminated, and the contact with the overlying layer is sharp, without an erosional surface. On the other hand, the lower contact is locally characterized by some erosion of P1A.

Unit P1B varies irregularly in thickness with distance from the source, for example, ranging from ~50 to ~7 cm at ~2 km from the volcano. This unit is, however, absent beyond 4.5 km from the crater. The relative limited dispersion of this unit, its irregular thickness, depositional structure (lamination), framework (matrix-supported), and grain type (juvenile and accidental lithic fragments) characteristics, as well as the nature of the lower and upper contacts, indicate that unit P1B is a low-concentration pyroclastic density current deposit.

P1C unit

Unit P1C consists of a blanket of clast-supported, white pumice lapilli. Juvenile lithic fragments are present with a typical content of 9 wt%. At most sites, we find that the maximum lithic size increases slightly upwards by 8 %, whereas pumice sizes do not change. The uppermost part of the deposit is often missing due to erosion in particular by the pyroclastic density currents of the 1902 eruption in the downwind direction.

Unit P1C has a maximum measured thickness of 100 cm at 3 km from the crater in the downwind direction, which steadily thins to ~25 cm within 5 km of the vent. In the cross-wind direction, unit P1C is 90-cm thick in the most proximal sections, thinning to > 25 cm within 4.5 km of the volcano. The relatively widespread nature of this deposit, its uniformly decreasing thickness with distance from the source, its framework (clast-supported), and grain type (pumice and juvenile lithic fragments) characteristics indicate that unit P1C is a fall deposit.

P1D unit

Unit P1D is a layer of fine brown ash containing crystals (plagioclases, pyroxenes), juvenile, and accidental lithic fragments. P1D deposits are ~30-cm thick at ~3 km from the volcano and are clearly absent beyond 4.5 km where unit P1C is overlain by a soil. Other deposits correlative to P1D have been identified by Westercamp and Traineau (1983a), Bardintzeff et al. (1989), and Traineau et al. (1989). Those are very poorly sorted ($\sigma_\phi = 3.75\phi$) layers of very fine ash containing rounded pumice lapilli and blocks up to 1 m in diameter. Bardintzeff et al. (1989) showed that the coarse ash fraction of the grain-size distribution is mostly made

of crystals (~65 wt%) and white pumice (~25 wt%) with minor juvenile and accidental lithic fragments (~10 wt%). The amounts of white pumice and lithic fragments reach ~70 and ~30 wt%, respectively, in the fine lapilli fraction of the grain-size distribution.

The very poorly sorted nature of this deposit, its valley-confined geometry (see section "Distribution of P1 deposits") and erosion of the underlying pumice fall unit (P1C) suggest that P1D is the deposit of a high-concentration pyroclastic density current. Whereas Bardintzeff et al. (1989) focused on the deposits of the dense basal layer of pyroclastic density currents (PDCs), we focus here on the deposits of the dilute upper layer of PDCs, which will be used to make quantitative inferences regarding eruption dynamics.

Distribution of P1 deposits

Figure 4 shows stratigraphic correlations of P1 outcrops along a SE–NW axis and a W–E axis. The complete sequence can be found up to 5 km from the volcano, in particular on the Grande Savane road (sites 10, 12, and 73 in Fig. 4) along an axis between the caldera and the town of Le Prêcheur (Fig. 1).

Our number of measured sections is not sufficient to draw isopach maps for the basal layers nor to quantitatively interpret these deposits in terms of eruption dynamics. However, isopach and isopleth maps of unit P1A confirm the direction of dispersal inferred by Traineau et al. (1989) (Figs. 5 and 6), which is characteristic of the wind profile above the Lesser Antilles (Traineau et al. 1989; Komorowski et al. 2008). The northwestern arms of our 10 and 50 cm isopachs of P1A are not well constrained due to a lack of outcrops in an area where dense tropical forest made the outcrops scarce, affected by intense weathering and very difficult to identify. Neither Traineau et al. (1989) nor Bardintzeff et al. (1989) found outcrops in this area. Not surprisingly, P1A and P1C have a similar direction of dispersal axis, although the southeastern arms of our three isopachs are not well constrained due to intense erosion by both 1902 products and current intensive farming.

P1B deposits are widespread on the SW flank of the volcano and vary between ~60 cm at 1 km from the volcano to a few centimeters near the coast (Fig. 5). On the other hand, the high-concentration PDC deposits associated with P1D are mainly concentrated in the Prêcheur and Sèche rivers (Fig. 5), as found by previous studies (Westercamp and Traineau 1983a, b; Bardintzeff et al. 1989; Traineau et al. 1989). We observed, however, that the low-concentration PDC deposits are present in the Grande Savane area (Fig. 5). The distribution of P1D deposits and topographical barriers around the volcano suggest that whereas the upper dilute current of the PDC directly flowed between Morne Plumé and Morne Vert Pré to fill the Grande Savane depression, the lower dense current diverged into the Prêcheur river valley (Fig. 5). The lack of low-concentration PDC deposit on the northern arm of the Prêcheur river supports the idea that the low-concentration PDC did not originate from the lower part of the river but probably detached from the dense region of the PDC near Mt Pelée's summit.

Grain-size distribution

Nine samples from the P1 unit were analyzed in order to determine the mean grain-size distribution for the lapilli fraction of P1A and P1C deposits (Table 1). The

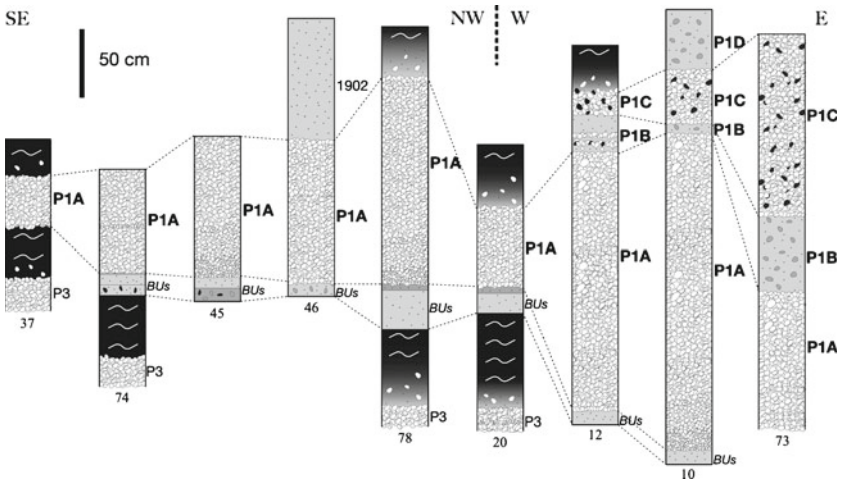

Fig. 4 Stratigraphic correlations along the St Pierre-Le Prêcheur (*SE to NW*) and Le Prêcheur-Caldera (*W to E*) profiles (see dotted line in Fig. 1). The complete P1 sequence can be found up to 5 km from the crater and is particularly visible along the Grande Savane road (from site 73 to site 20)

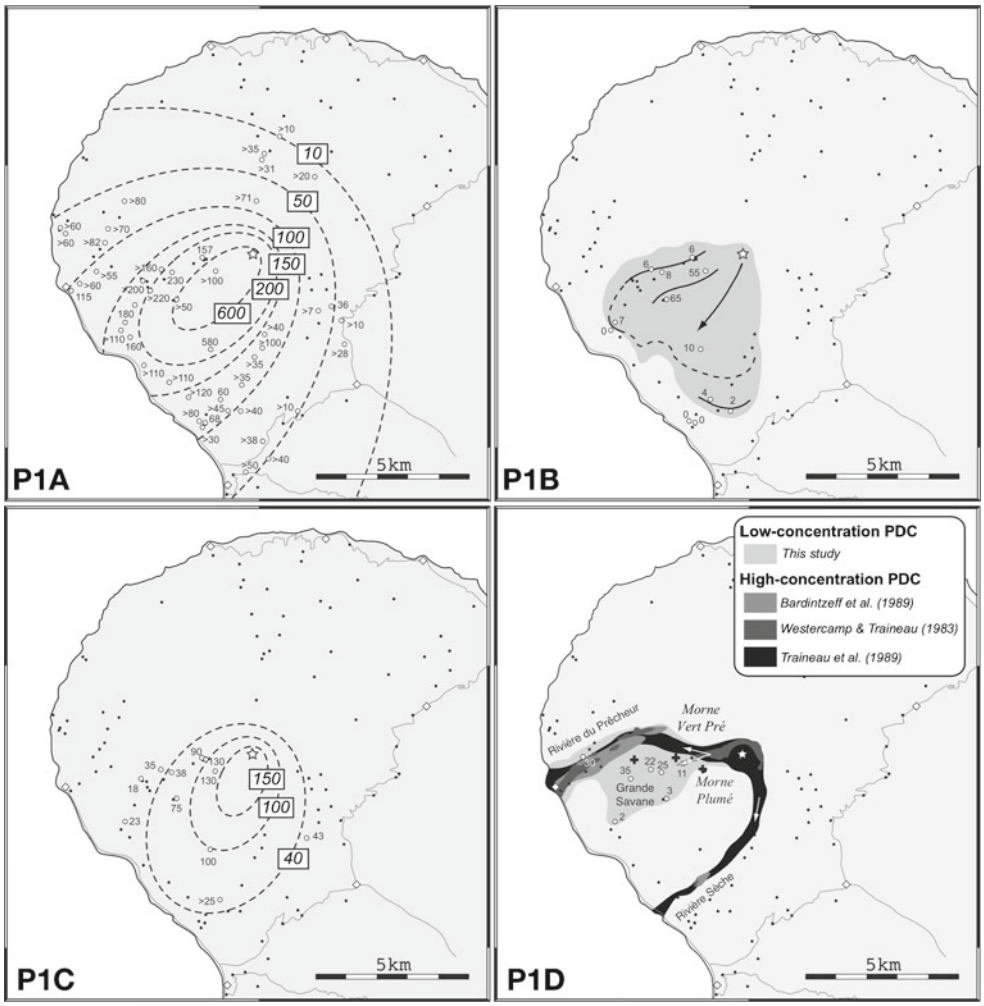

Fig. 5 Isopach maps (in centimeters) for P1A, P1B, P1C, and P1D. Measured sample locations are indicated by *open circles*. Where unit P1B is missing, a fine-grained limit is observed between P1A and P1C (thickness = 0 in the *upper right map*). *Black crosses* in the *lower right map* give the location of the main topographical barriers including Morne Plumé and Morne Vert Pré. Direction of dispersal axes for P1A and P1C are consistent with local wind profiles

purpose of this analysis is to estimate the amount of gas trapped in pumice fragments (see section "Grain size sampling and seiving"). A detailed analysis of the nature and origin of crystals and lithic fragments contained in the deposits is beyond the scope of this paper and can be found in Bardintzeff et al. (1989).

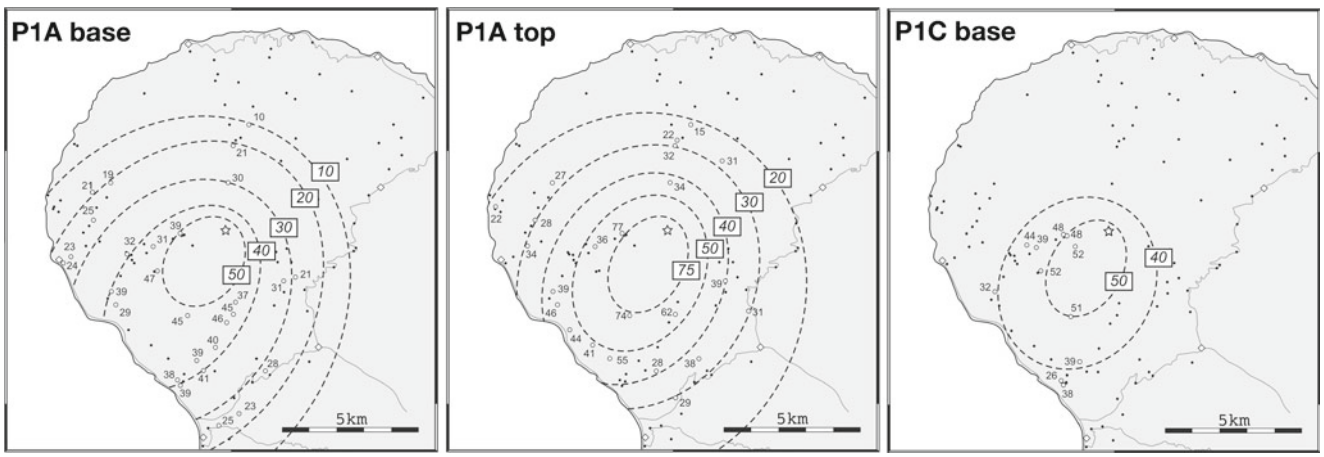

Fig. 6 Isopleth maps (in millimeters) for the lithic fragments sampled at the base and the top of P1A and the base of P1C. Measured sample locations are indicated by *open circles*. Direction of dispersal axes are consistent with those inferred from the isopach maps for P1A and P1C

Table 1 Sampling of pumice fall deposits for grain-size analysis

Sample	Site	Unit	Subunit	Altitude (m)	Distance from the vent (km)	Thickness (cm)
1	10	P1A	base	570	2.75	230
2	10	P1A	top	570	2.75	230
3	10	P1C	base	570	2.75	38
4	47	P1A	base	100	5.20	120
5	47	P1A	top	100	5.20	120
6	101	P1A	bulk	160	4.75	180
7	101	P1A	base	160	4.75	180
8	101	P1A	top	160	4.75	180
9	101	P1C	base	160	4.75	23

From our analysis, we infer that the power law coefficient D defined in section "Grain-size sampling and sieving" increased during the eruption from $D = 3.19$ for early P1A to $D = 3.33$ for late P1A and early P1C (Fig. 7). As we will describe below, the evolution of this parameter can be interpreted as an increase in ash production (Kaminski and Jaupart 1998).

Eruptive parameters

Volume of P1 deposits

Various methods can be used to assess the volume of pumice fall deposits emitted during an explosive eruption (Bonadonna and Costa 2012). However, on small tropical islands where only proximal and, furthermore, incompletely preserved deposits are available, volume calculations are bound to provide minimum estimates only.

Figure 8a gives the thinning behavior of P1A and P1C based on our isopach maps, which is commonly

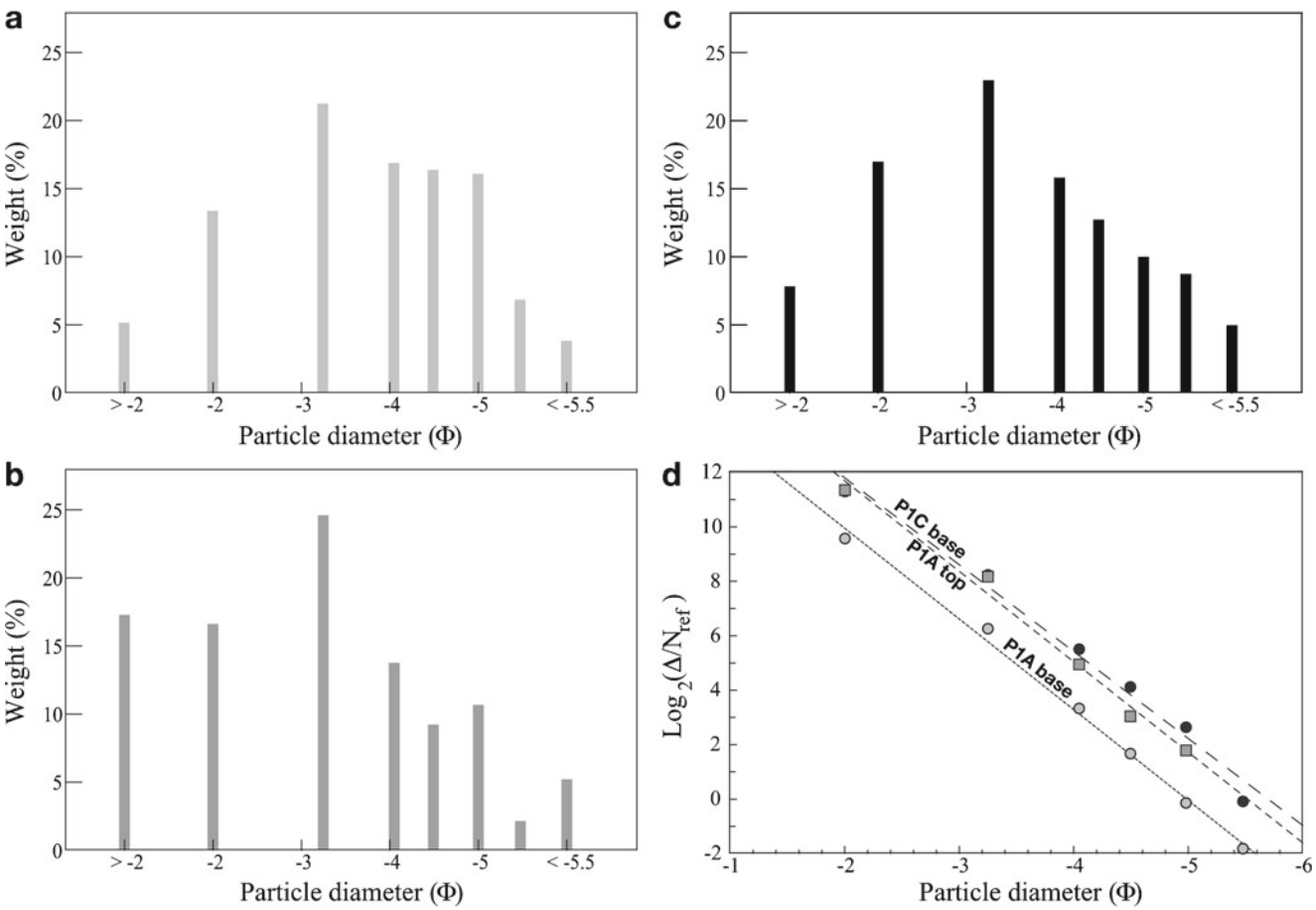

Fig. 7 Mean grain-size distribution for the lapilli fraction of **a** the base of P1A, **b** the top of P1A, and **c** the base of P1C in a classical particle diameter (ϕ) vs. frequency (in weight percent) histogram. **d** Same grain-size distributions reported as the number of fragments in each sieve class Δ normalized by an arbitrary constant N_{ref}, as a function of size (in ϕ units). *Light gray circles*, *dark gray squares*, and *solid circles* correspond to data for P1A base, P1A top, and P1C base, respectively. *Dotted*, *dashed*, and *long dashed lines* correspond to best linear fits to the data for P1A base ($D = 3.19$), P1A top ($D = 3.33$), and P1C base ($D = 3.33$), respectively. In this plot, the value of D corresponds to the slope of the best linear fit

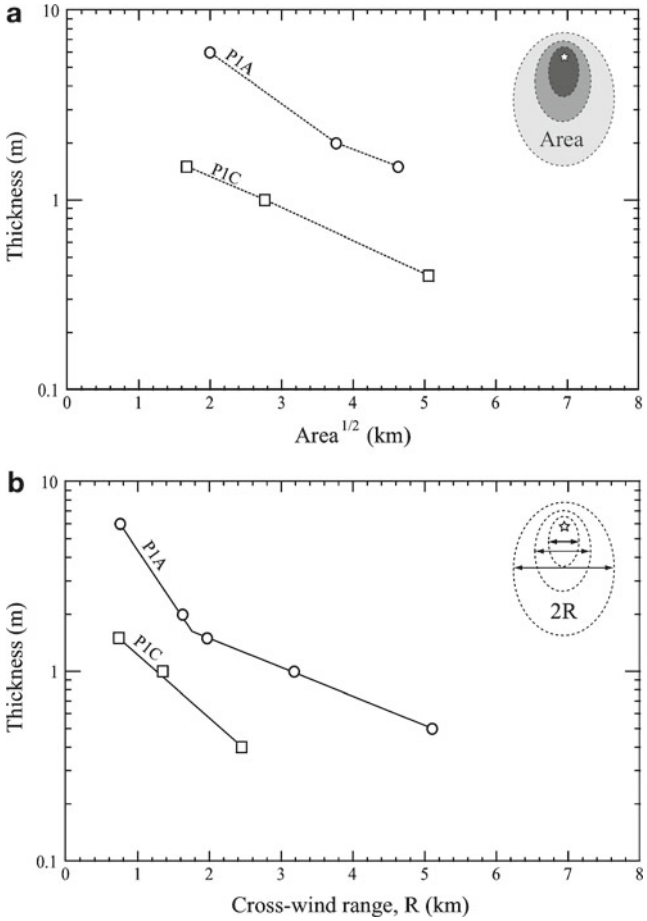

Fig. 8 Deposit thinning profiles generated from the isopach maps for P1A and P1C. **a** Semi-log thickness-square root of isopach area plot. **b** Semi-log thickness-crosswind range *R* (in kilometers). In both panels, *open circles* correspond to P1A, whereas *open squares* correspond to P1C. *Solid lines* in **b** are extrapolated fits

used to infer the volume of the fall units. Only three measurements are reported for P1A since the 10, 50, and 100 cm isopachs are not constrained in the ocean. The method of Fierstein and Nathenson (1992) cannot be used on this dataset because the break-in slope corresponding to the transition from the column to the umbrella domain is not clearly defined (Fig. 8a). The minimum volume of P1A is found to be 0.12 and 0.10 km^3 using the method of Pyle (1989) and Legros (2000), respectively, whereas the minimum volume of P1C is found to be 0.04 km^3 using both techniques. The cumulative minimum volume of the fall units is thus 0.15 km^3 (0.06 km^3 DRE[1]), which corresponds to a total mass of 1.6×10^{11} kg (75 wt% from P1A and 25 wt% from P1C).

[1]This is based on a magma density of 2,400 kg m^{-3} and a deposit density of 1,000 kg m^{-3} (Traineau et al. 1989).

The volume of PDC deposits is more difficult to assess. Here, we use the observed relationship between the area covered by low-concentration PDCs and their volume (Dade and Huppert 1998; Calder et al. 1999). From Fig. 5, we estimate inundated areas of 21 km^2 for P1B and 9 km^2 for the dilute PDC of P1D. Using the approach illustrated in Fig. 1a of Calder et al. (1999), we estimate a volume of 0.006 km^3 DRE for the low-concentration PDC of P1B, which corresponds to a mass of deposit of 1.5×10^{10} kg, and a volume of 0.003 km^3 DRE for the dilute PDC of P1D, which corresponds to a mass of deposit of 7.2×10^9 kg. The latter value is only a small fraction of the total mass of P1D since the dense part of the PDC deposits confined in the Prêcheur and Sèche rivers is estimated to be 2×10^{11} kg (Traineau and Westercamp 1985).

The total minimum mass of magma erupted during the violent explosive phase of P1 (P1A to P1D) is found to be $\sim 4 \times 10^{11}$ kg, which corresponds to a VEI-4 event (Newhall and Self 1982) with a magnitude of 4.6 (Pyle 1995). Although only minimum volumes are available for the fall units, our calculations indicate that the P1 eruption is a small Plinian event with a maximum column height lower than 25 km (Newhall and Self 1982).

Column height (P1A and P1C)

The altitude reached by a volcanic column depends on several factors including the mass flow rate and the strength of winds (Carey and Sparks 1986; Bursik 2001). In the Lesser Antilles, northeasterly trade and lower stratospheric winds dominate at low (< 11 km) and high (> 21 km) altitudes, whereas southwesterly antitrade winds persist at mid-altitude (11–21 km) (Traineau et al. 1989). In order to improve estimations of maximum column height in a bidirectional wind profile, we use the version of the model of Carey and Sparks (1986) adapted to the El Chichon area (Carey and Sigurdsson 1989) considering that the intensity of trade winds increases linearly from 0 to 25 m s^{-1} up to an altitude of 11 km, whereas antitrade winds blow in the opposite direction between 11 and 21 km increasing linearly up to 20 m s^{-1}. Those imposed wind speeds and directions are consistent with current measurements above the Lesser Antilles (Komorowski et al. 2008). Our isopleth maps (Fig. 6) in this framework yield a maximum height of 19.1 ± 0.9 km for the beginning of P1A, 21.9 ± 2.0 km for the end of P1A, and 19.9 ± 0.2 km for the beginning of P1C. Error bars are calculated using the three values of maximum height inferred from the 8, 16, and 32-mm isopleths (see Fig. 17 in Carey and Sigurdsson 1989).

An alternative method to estimate the altitude reached by the volcanic column consists in using the break-in slope in the log(thickness) vs area$^{1/2}$ plot (Fig. 8a). Since this break-in slope is not constrained in Fig. 8a, we use the break-in slope obtained in the log(thickness) vs cross-wind range plot (Fig. 8b), which is well constrained on land and insensitive to wind speed. Note that the two break-in slopes are not independent since the area is imposed by the cross-wind and downwind ranges, but because we are lacking downwind range values, it is best to work with cross-wind ranges. For P1A, our data show that $R_{cb} = 1.7$ km, whereas for P1C, one can only assess that $R_{cb} > 2.5$ km (Fig. 8b). These values correspond to the radial position of the plume corner at an altitude corresponding to the base of the umbrella cloud (H_{cb}), which is slightly different from the column radius at the level of neutral buoyancy (H_b) (see Fig. 1 in Bonadonna and Phillips (2003)). Thus, we use Eq. (2) of Bonadonna and Phillips (2003) to convert R_{cb} to a column radius at the neutral buoyancy height ($R_b = R_{cb}/0.8$), which is then converted to column height (H_t) using a model for the volcanic column (e.g., Sparks 1986).

Since the geometry of the column is mainly imposed by the amount of atmospheric air engulfed during ascent, we use our 1-D model (Carazzo et al. 2008a), which incorporates a detailed description of the process of turbulent mixing.[2] This model yields an average column height of 18.5 ± 1 km for P1A and $> 20 \pm 1$ km for P1C. The models of Sparks (1986) and Woods (1988) yield 10 and 16.5 km for P1A, and > 13 and > 20 km for P1C, respectively. The differences between our predictions and those made with the model of Woods (1988) are mainly due to the use of different descriptions for the process of turbulent mixing (Carazzo et al. 2008a), whereas the predictions made with the model of Sparks (1986) are affected by the lack of a detailed description for the evolution of the thermal energy in the plume (Woods 1988).

Fountain height (P1D)

The height of the volcanic fountain feeding the eruption during P1D can be inferred using the model of Doyle et al. (2010). Using a two-layer model for propagation of dense and dilute regions of pyroclastic density currents, they show that the runout distance of the upper dilute current (L) is mainly imposed by fountain height (H_F). Their results can be summarized in a parametric equation (their Eq. 4),

$$H_F \approx 2.2 \left(\frac{d_p}{\epsilon_p}\right)^{1/4} L^{3/4}, \quad (3)$$

where ϵ_p is the initial volume fraction of particles, and d_p is the mean particle diameter. A plausible range of values for ϵ_p can be taken as $5 \times 10^{-3} - 10^{-2}$ (Doyle et al. 2010), and the runout distance is observed to be $L \approx 4.5$ km for the dilute PDC deposits located in the Grande Savane depression (Fig. 5). Grain-size analyses show that d_p varies in the range of 0.125–64 mm within P1D deposits (Bardintzeff 1985). The mean diameter is found to be $d_p = 5.65$ mm, and the fountain height during P1D is estimated to be $H_F \approx 1.3 \pm 0.1$ km based on uncertainties on ϵ_p.

Intensity of P1A and P1C

Using the classical method of Sparks (1986) to estimate the mass discharge rates associated with the maximum column heights inferred from the model of Carey and Sparks (1986), we obtain maximum discharge rates of $2 \pm 0.8 \times 10^7$ kg s^{-1} for the beginning of P1A, $3.6 \pm 1.6 \times 10^7$ kg s^{-1} for the end of P1A, and $2.5 \pm 1.1 \times 10^7$ kg s^{-1} for the beginning of P1C.

We also used the refined model of Carazzo et al. (2008a) to estimate mean discharge rates from mean column heights constrained in section "Column height (P1A and P1C)". We obtain mean discharge rates of $1.6 \pm 0.5 \times 10^7$ kg s^{-1} for the entire P1A phase and $> 3.4 \pm 0.5 \times 10^7$ kg s^{-1} for the entire P1C phase,[3] implying that the eruption probably increased in intensity during P1C.

A third estimate can be obtained using more sophisticated sedimentation models (Bursik et al. 1992; Bonadonna and Phillips 2003). Ideally, we would use the model of Bonadonna and Phillips (2003) which accounts for the effect of wind on particle sedimentation. However, because there are not enough data to constrain isopachs along the dispersal axis, we use the sedimentation model of Bursik et al. (1992) together with data shown in Fig. 8b. Using Eq. 15 of Bursik et al. (1992), the thinning behavior of the cross-wind range can thus be used to infer the volumetric flow rate of the umbrella cloud (Q_b) with no assumption on the maximum height.

[2] Calculations are made using a top-hat formalism (Morton et al. 1956). Top-hat values of column radius can be converted to real (Gaussian) values by using $R_{model} = \sqrt{2} R_{real}$.

[3] Calculations have been made for tropical atmospheric conditions and for a crystal-bearing rhyolitic magma (andesitic bulk composition) with an initial temperature of 1,173 K (Martel et al. 1998) and a bulk density of 2,400 kg m^{-3}.

Figure 9a shows that the best model fit to P1A data is for $Q_b = 6 \times 10^9$ kg s^{-1}. Calculations have been made using our grain-size distribution for P1A together with the formulae of Bonadonna et al. (1998) for the particle settling velocities. Although the result is highly sensitive to the grain-size distribution used, the lack of fine particles in our grain-size distribution does not affect our predictions simply because fine particles missing in the model are also missing in the field (proximal region). Moreover, the good fit to the power-law of the grain-size distribution (Fig. 7a) is a strong indication that the distribution obtained for large sizes will still apply to finer sizes, as shown in Kaminski and Jaupart (1998). By volume conservation between the neutral buoyancy height and the umbrella cloud (Carey and Sparks 1986), one can deduce the mass discharge rate feeding the eruptive column by using the model of Carazzo et al. (2008a). This method yields mean source discharge rates of $3 \pm 0.5 \times 10^7$ kg s^{-1} for P1A (Fig. 9b), quite consistent with those obtained above.

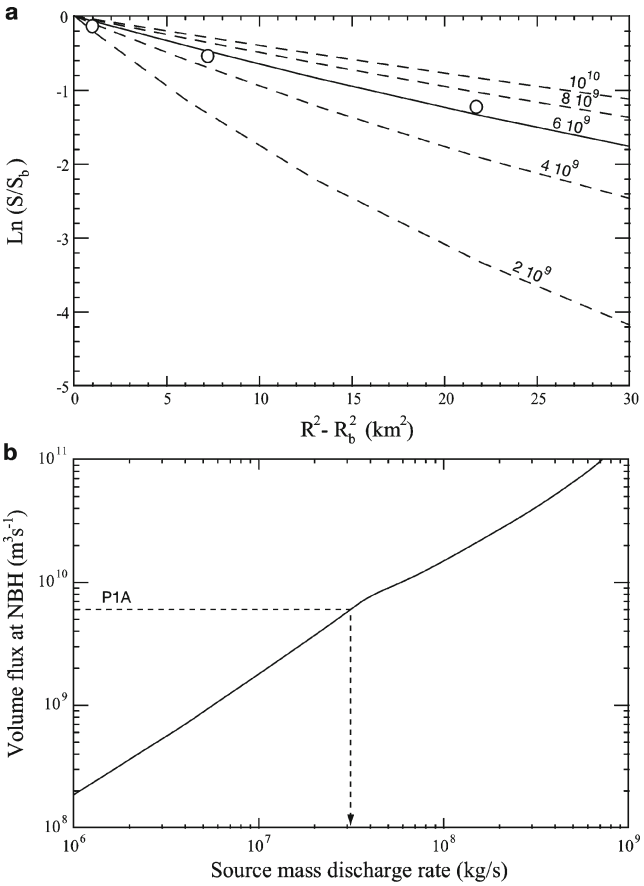

Fig. 9 Mass discharge rates inferred from the models of Bursik et al. (1992) and Carazzo et al. (2008a). **a** Variation of sedimentation rate with distance from the vent for different volumetric flow rates of the umbrella cloud Q_b (in cubic meters per second). S is the total mass of particles accumulated per unit length, and S_b is the mass accumulation rate per unit length at the column/umbrella corner (R_b) (Bursik et al. 1992). *Solid curve* gives the best fit to the data for P1A corresponding to $Q_b = 6 \times 10^9$ kg s^{-1}. **b** Volumetric flux rate feeding the umbrella cloud (in cubic meters per second) as a function of the source mass discharge rate released at the volcanic column base (in kilograms per second)

Intensity of P1B and P1D

The intensity of the eruption during the partial and final collapse phases is more difficult to estimate. In general, mass discharge rates are calculated from runout distances observed in the field using the model of Bursik and Woods (1996), which treats pyroclastic flows as dilute suspensions. Doyle et al. (2010) showed recently that this assumption is valid for tall, fine-grained column collapses, for which the flow slowly transfers its mass to the dense basal flow. We consider that the model of Bursik and Woods (1996) is relevant for the ash-cloud surge of P1D, but not the pumice-rich flow. Assuming that the dilute PDC behaved as a supercritical flow (i.e., fast (100–200 m s^{-1}) and shallow (500–1,000 m)) entraining air as it propagated, we find a mass flux of $9 \pm 3 \times 10^7$ kg s^{-1}. This value does not take into account topographic slopes. Doyle et al. (2010) showed, however, that the runout distance of the upper dilute current mostly depends on the initial fountain height (Eq. 3), which is imposed by the mass discharge rate, rather than by ground slopes. It is therefore likely that theoretical uncertainties are accounted for within the large error bars on the mass discharge rate for P1D. Finally, although the dilute PDC deposit of P1B was emplaced by a different mechanism than the dilute PDC deposit of P1D, the same assumption about the supercritical nature of the flow can be made. In Fig. 5, we estimate a similar maximum runout distance of 4.5 km, which gives a mass discharge rate of the same order of magnitude as that of P1D (i.e., $9 \pm 3 \times 10^7$ kg s^{-1}).

The Plinian plume/pyroclastic fountain transition

Theoretical models of explosive eruptions predict that the eruptive regime is governed by the velocity, mass discharge rate, and exsolved gas content (Wilson et al. 1980). Mass fluxes calculated for each eruptive phase either from the maximum column heights inferred from the distribution of the deposits, or from the maximum runout distances, show a progressive increase of eruptive intensity over time, which is consistent with the observed evolution of pumice size (inverse grading of P1A) and maximum lithic size and content (P1A to P1C) at all outcrops of P1 (section "Stratigraphy"). This

Table 2 Gas contents and deduced exit velocities

Unit	n_0 (wt%)	α_c	x_0 (wt%)	x_f (wt%)	x_e (wt%)	U_{free} (m s^{-1})	U_{min} (m s^{-1})
P1A[a]	5.80	49	2.96	2.07	1.24	154	148
P1A[b]	5.80	54	2.66	1.86	1.39	163	165
P1C[a]	5.80	56	2.57	1.80	1.35	160	165
P1D	5.50	58	2.31	1.62	*1.5*	–	165

n_0 is the total volatile content of the melt (Martel et al. 1998), α_c is the percentage of crystals in the melt plus lithics in the flow (Martel et al. 1998; Bardintzeff et al. 1989), x_0 is the mass fraction of gas in the magma assuming complete degassing, x_f is the mass fraction of exsolved gas in the gas+pyroclasts mixture at fragmentation for a threshold vesicularity of 70 %, x_e is the effective amount of exsolved gas at the volcanic column base (Kaminski and Jaupart 1998), U_{free} is the supersonic velocity after free decompression calculated using x_e, U_{min} is the eruptive velocity deduced from the distribution of the lithic fragments. See Supplementary Information for more details
[a]At base (early stage)
[b]At top (late stage)

result is quite classical and similar to other powerful eruptions (Wilson et al. 1980).

Amounts of volcanic gas in the eruptive mixture at the vent must be known or inferred in order to assess the transition from a convecting to a collapsing eruption column, but are difficult to quantify. Magmatic water contents in glass inclusions (n_0) are found to be 5.8 ± 0.7 wt% in the pumice fallout units (P1A and P1C) and 5.5 ± 1.5 wt% in the pumice-rich flow unit (P1D) (Martel et al. 1998). Correcting the volatile concentration for the presence of crystals and lithics, which do not contain volatiles, we find that the initial gas content in the magma decreased from 2.96 to 2.31 wt% during the eruption (Table 2). As in Kaminski and Jaupart (2001), we calculate x_f, the mass fraction of exsolved gas in the mixture at fragmentation level for a threshold vesicularity of 70 % (Table 2), which assumes closed-system conditions consistent with degassing models for P1 (Villemant and Boudon 1998; Martel et al. 1998; Villemant and Boudon 1999; Martel et al. 2000). The effective amount of exsolved gas at the base of the volcanic column (x_e) can differ from x_f due to gas entrapment by pumices as a function of their size distribution (Kaminski and Jaupart 1998). Using the power law coefficient D estimated in section "Grain size distribution", we calculate x_f for P1A and P1C (Table 2).

The estimation of x_e for P1D is more difficult because we were unable to determine D for these deposits. Alternatively, we used a theoretical model simulating the decompression of a volcanic mixture (Woods and Bower 1995) together with scaling laws valid for turbulent fountains (Carazzo et al. 2010) to infer a value for x_e (see Supplementary Information). Our results give $x_e = 1.5$ wt% (Table 2).

Figure 10a compares the predictions of column collapse using the model of Carazzo et al. (2008b) with the values of mass discharge rate and effective gas content in the column for P1. The P1 eruption started in the region of stable convective plumes but the mass

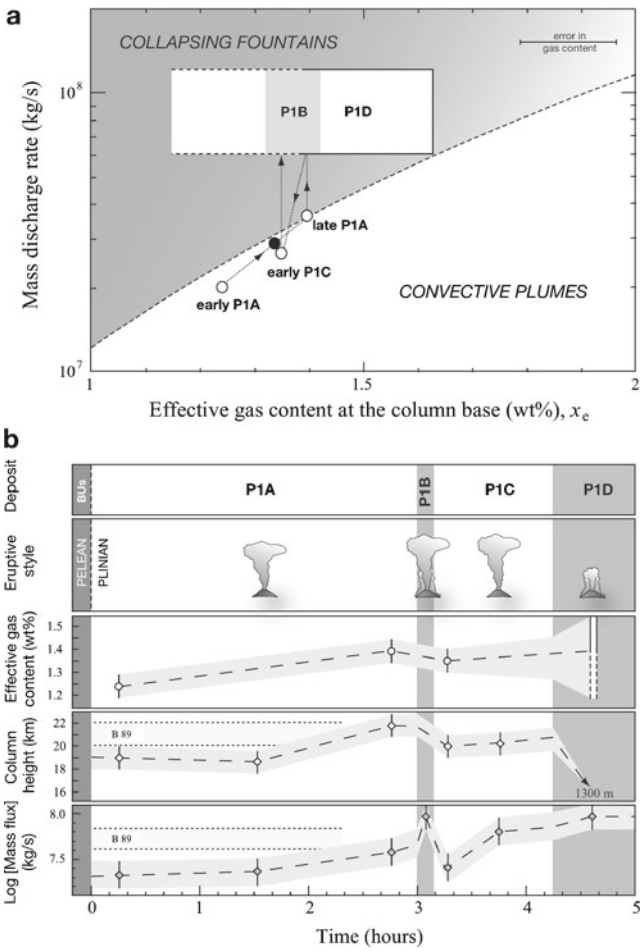

Fig. 10 **a** Transition diagram depicting the P1 eruptive events and depositional units. *Dotted curve* corresponds to the maximum mass discharge rate feeding a column before collapse as a function of the effective gas content at the column base (Carazzo et al. (2008b)'s model for a tropical atmosphere). *Open circles* correspond to geological data inferred for the P1A and P1C, whereas the *large open square* gives the range of possible values for P1B and P1D. Mean discharge rates for P1A is reported as a *solid circle* (the amount of gas is interpolated to fit on the *arrow*). **b** Summary of the eruptive parameters calculated for P1. The results of Bardintzeff et al. (1989) are reported as B89. See Supplementary Information for duration calculation

discharge rate increased slowly during P1A. Concurrently, fragmentation produced finer grained pumice (i.e., higher D), increasing the amount of free exsolved gas in the volcanic mixture and tending to maintain the eruption in the convective plume field. During P1A, the eruption was evolving close to the plume/fountain transition, where the flow behavior becomes more sensitive to small variations of gas content, mass flux, and grain-size distribution of pyroclasts. P1B deposits must have been produced by a partial collapse of the column resulting from an increase in mass discharge rate. Total collapse occurred an hour later (end of P1C) because of the combination of a decrease of effective gas content and greater mass flux. The increase of mass flux probably resulted from the erosion of the volcanic conduit, as suggested by the relatively constant eruptive velocities (Table 2) and an increase in lithic fragment content in the deposits of P1C. During the final collapse, which produced P1D deposits, it is clear from Fig. 10b that the eruption reached its maximum mass flux, but the evolution of the effective gas content is unclear.

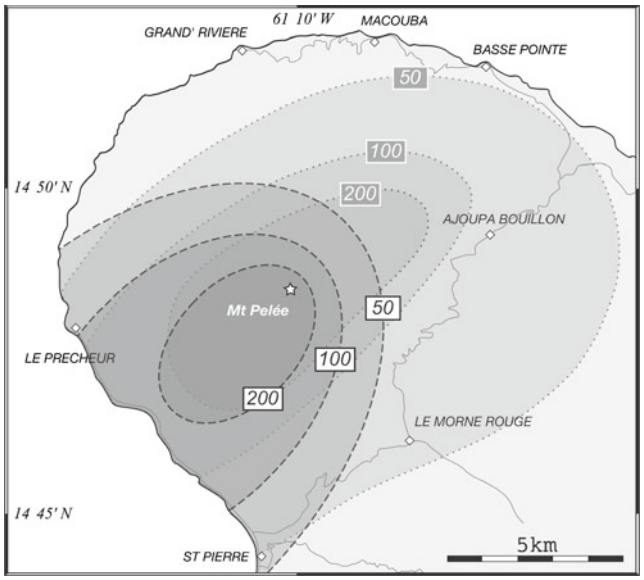

Fig. 11 Comparison between isopach maps (in centimeters) of Traineau et al. (1989) (*light gray dotted areas*) and of this study (*dark gray dashed areas*). The main difference is the dispersion of the pumice fall deposits to the east and northeast of the volcano, which we interpret as belonging to the P2 eruptive sequence

Discussion

Comparison with previous studies

Isopach maps of the P1A deposit are not consistent between Traineau et al. (1989)'s work and our study (Fig. 11). We interpret some of the deposits to the E and the NE of Mt Pelée, attributed to P1 by Traineau et al. (1989), as belonging to the P2 sequence (AD 280 eruption). The two latest pumice eruptions at Mt Pelée (P1 and P2) indeed have similar depositional sequences, but contrary to P1A, which is inversely graded, the lower pumice fall unit of the P2 eruption is ungraded. Moreover, the uppermost part of P2 pumice fall deposit exhibits slight stratification in pumice size, which is absent in P1C. Pumice fall deposits to the NE of the volcano not only have the characteristic stratigraphy of P2 but also overlie a thin palaeo-soil on top of P3 deposits, strongly contrasting with thick palaeosoils to the SW of the volcano (Fig. 4). This observation is consistent with the relatively short time interval between P3 and P2 (~340 years) compared to a much longer interval between P3 and P1 (~1,360 years). The interpretation of Traineau et al. (1989) would imply complete erosion of P2 in that region, which is unlikely.

The P1 pumice fall is, as a consequence, also calculated to be less voluminous than in Traineau et al. (1989). Whereas Traineau et al. (1989) give a minimum volume of 0.70 ± 0.25 km^3 based on the methods of Walker (1980) and Froggat (1982), our calculations provide a minimum volume of 0.15 km^3 for P1A and P1C. We note, however, that using the method of Legros (2000) on the 200-cm isopach of Traineau et al. (1989) would yield a minimum volume of 0.2 km^3. The disagreement between our study and Traineau et al. (1989)'s work is thus clearly due to our reinterpretation of the deposits to the E and the NE flanks of Mt Pelée as apparent in Fig. 11.

Column heights for P1 inferred from our field study vary within a narrow range (19–22 km) equivalent but broader than that (20–22 km) proposed by Bardintzeff et al. (1989) based on their calculation of mass eruption rate. The range in mass discharge rate feeding the eruption during the stable column stage proposed by Bardintzeff et al. (1989) on the basis of assumptions about the vent radius ($3.8–7\times10^7$ kg s^{-1}) is, however, greater than our estimations for P1A ($2–3.6\times10^7$ kg s^{-1}) and P1C ($2.5–3.4\times10^7$ kg s^{-1}). This disagreement is likely to be due to the different techniques used. Whereas Bardintzeff et al. (1989) use the formula of Wilson et al. (1980) together with assumptions about the vent radius, water content, temperature, and magma viscosity, our estimations are based on our field data together with an array of more recent physical models (Carey and Sparks 1986; Sparks 1986; Carey and Sigurdsson 1989; Bursik et al. 1992; Bursik and

Woods 1996; Bonadonna and Phillips 2003; Carazzo et al. 2008a; Doyle et al. 2010).

The duration of the eruption also differs between Bardintzeff et al. (1989)'s study and ours. Whereas Bardintzeff et al. (1989) calculate a duration of 1.5–3 h based on their total volume and mass eruption rate, we find by using the same method together with mean mass discharge rates that P1 probably lasted longer (∼5 h). The true duration of this eruption is nevertheless difficult to assess because the calculated volumes are minimum values (see Supplementary Information).

Type of column collapse

The transition from a sustained column to a collapsing fountain usually occurs when the eruption intensity increases strongly and/or when the amount of gas in the column decreases (Carey and Sigurdsson 1989). The P1 eruption at Mt Pelée volcano is characterized by an evolution close to the plume/fountain transition as observed in numerical simulations (Neri et al. 2002; Di Muro et al. 2004) and inferred from field observations of other fall deposits (Di Muro et al. 2008). In this transitional regime, the eruptive column underwent the competing effects of the stabilizing increase in gas content and the destabilizing increase in mass discharge rate. The unusual evolution of the effective amount of gas during the P1 eruption prevented column collapse for a few hours, but such a marginally stable evolution is particularly problematic for hazard assessment, and further investigations are required to determine whether this behavior is systematic of Mt Pelée volcano eruptions. In particular, the study of the P2 AD 280 eruption should help in achieving this goal.

Conclusion

New field data allow a reconstruction of a detailed time evolution of the P1 eruption and of the mechanisms controlling the eruptive dynamics. Our interpretation differs from those in previously published studies mainly because of re-interpretation of deposits on the E and the NE flanks of the volcano. From our field study and physical modeling, we find that P1 was a small Plinian eruption (VEI-4, M=4.6) evolving close to the plume/fountain transition. The total volume of tephra is estimated to be > 0.15 km^3, and the mass eruption rate increased from 2×10^7 to $> 6 \times 10^7$ kg s^{-1} during probably ∼5 h.

After an initial dome-forming stage (Villemant et al. 1996; Villemant and Boudon 1998, 1999), the eruption produced a 19–22-km-high stable column, which dispersed pumice and ash over the SW flank of the volcano for ∼3 h (P1A). Combined increases in mass discharge rate and effective gas content due to more efficient fragmentation led to partial collapse of the column with an associated dilute PDC (P1B). The plume height then reached a maximum of 20 km (P1C) for ∼1 h before collapse resulting in the formation of a ∼1.3-km-high fountain feeding PDCs for less than an hour.

This study provides a detailed reconstruction of the most recent Plinian eruption at Mt Pelée volcano, which was characterized by an evolution close to the plume/fountain transition and a final column collapse. The two most recent pumice eruptions (P1 and P2) have similar depositional sequences, suggesting that this marginally stable behavior might be recurrent at Mt Pelée volcano. Therefore, the need for a better understanding of other eruptions in Martinique is crucial. This study provides a framework for assessing specific hazards in the Lesser Antilles.

Acknowledgements This paper has been much improved thanks to T. Thordarson, C. Bonadonna, and an anonymous reviewer. The authors acknowledge G. Boudon, J.C. Komorowski, and C. Martel for fruitful discussions; V. Clouard, S. Bazin, and the staff of the Mt Pelée observatory (OVSM) for their help. Support was provided by the Institut National des Sciences de l'Univers (INSU-CNRS) and the CASAVA Project (ANR-09-RISK-002). G. C. was partially supported by the Canadian Institute for Advance Research. J. G. was partially supported by a grant from the National Science Foundation (EAR-0711043).

References

Bardintzeff JM (1985) Les nuées ardentes: pétrogenèse et volcanologie. PhD thesis, Université Paris-Sud Orsay

Bardintzeff JM, Miskovsky JC, Traineau H, Westercamp D (1989) The recent pumice eruptions of Mt. Pelée, Martinique. Part II: Grain-size studies and modelling the last Plinian phase P1. J Volcan Geotherm Res 38:35–48

Bonadonna C, Costa A (2012) Estimating the volume of tephra deposits: a new simple strategy. Geology doi:10.1130/G32769.1

Bonadonna C, Phillips JC (2003) Sedimentation from strong volcanic plumes. J Geophys Res 108:2340

Bonadonna C, Ernst CGJ, Sparks RSJ (1998) Thickness variations and volume estimates of tephra fall deposits: the importance of particle Reynolds number. J Volcan Geotherm Res 81:173–187

Bourdier JL, Boudon G, Gourgaud A (1989) Stratigraphy of the 1902 and 1929 nuée-ardente deposits, Mt. Pelée, Martinique. J Volcan Geotherm Res 38:77–96

Bursik M (2001) Effect of wind on the rise height of volcanic plumes. Geophys Res Lett 28:3621–3624

Bursik M, Carey S, Sparks RSJ, Gilbert J (1992) Sedimentation of tephra by volcanic plumes. I. Theory and its comparison with a study of the Fogo A Plinian deposit, Sao Miguel (Azores). Bull Volcanol 54:329–334

Bursik MI, Woods AW (1996) The dynamics and thermodynamics of large ash flows. Bull Volcanol 58:175–193

Calder ES, Cole PD, Dade WB, Druitt TH, Hoblitt RP, Huppert HE, Ritchie L, Sparks RSJ, Young SR (1999) Mobility of pyroclastic flows and surges at the Soufriere Hills Volcano, Montserrat. Geophys Res Lett 26:537–540

Carazzo G, Kaminski E, Tait S (2008a) On the rise of turbulent plumes: quantitative effects of variable entrainment for submarine hydrothermal vents, terrestrial and extra terrestrial explosive volcanism. J Geophys Res 113:458. doi:10.1029/2007JB005

Carazzo G, Kaminski E, Tait S (2008b) On the dynamics of volcanic columns: a comparison of field data with a new model of negatively buoyant jets. J Volcanol Geotherm Res 178:94–103

Carazzo G, Kaminski E, Tait S (2010) The rise and fall of turbulent fountains: a new model for improved quantitative predictions. J Fluid Mech 657:265–284. doi:10.1017/S002211201000145X

Carey S, Sigurdsson H (1989) The intensity of Plinian eruptions. Bull Volcanol 51:28–40

Carey S, Sparks RSJ (1986) Quantitative models of the fallout and dispersal of tephra from volcanic eruption columns. Bull Volcanol 48:109–125

Dade WB, Huppert HE (1998) Long runout rockfalls. Geology 26:803–806

Di Muro A, Neri A, Rosi M (2004) Contemporaneous convective and collapsing eruptive dynamics: the transitional regime of explosive eruptions. Geophys Res Lett 31:L10,607

Di Muro A, Rosi M, Aguilera E, Barbieri R, Massa G, Mundula F, Pieri F (2008) Transport and sedimentation dynamics of transitional explosive eruption columns: the example of the 800 BP Quilotoa Plinian eruption (Ecuador). J Volcanol Geotherm Res 174:307–324

Doyle EE, Hogg AJ, Mader HM, Sparks RSJ (2010) A two-layer model for the evolution and propagation of dense and dilute regions of pyroclastic currents. J Volcanol Geotherm Res 190:365–378

Dupuy C, Dostal J, Traineau H (1985) Geochemistry of volcanic rocks from Mt. Pelée, Martinique. J Volcanol Geotherm Res 26:147–165

Fierstein J, Nathenson M (1992) Another look at the calculation of fallout tephra volumes. Bull Volcanol 48:109–125

Froggat PC (1982) Reviews of methods of estimating rhyolitic tephra volumes: applications to the Taupo volcanic zone, New Zealand. J Volcanol Geotherm Res 14:301–318

Kaminski E, Jaupart C (1998) The size distribution of pyroclasts and the fragmentation sequence in explosive volcanic eruptions. J Geophys Res 103:29,759–29,779

Kaminski E, Jaupart C (2001) Marginal stability of atmospheric eruption columns and pyroclastic flow generation. J Geophys Res 106:21,785–21,798

Komorowski JC, Legendre Y, Caron B, Boudon G (2008) Reconstruction and analysis of sub-plinian tephra dispersal during the 1530 AD Soufriere (Guadeloupe) eruption: implications for scenario definition and hazards assessment. J Volcanol Geotherm Res 178:491–515

Lacroix A (1904) La Montagne Pelée et ses éruptions. Masson, Paris

Legros F (2000) Minimum volume of a tephra fallout deposit estimated from a single isopach. J Volcanol Geotherm Res 96:25–32

Martel C, Poussineau S (2007) Diversity of eruptive styles inferred from the microlites of Mt. Pelée andesite (Martinique, Lesser Antilles). J Volcanol Geotherm Res 166:233–254

Martel C, Pichavant M, Bourdier J-L, Traineau H, Holtz F, Scaillet B (1998) Magma storage conditions and control of eruption regime in silicic volcanoes: experimental evidence from Mt. Pelée. Earth Planet Sci Lett 156:89–99

Martel C, Bourdier JL, Pichavant M, Traineau H (2000) Textures, water content and degassing of silicic andesites from recent Plinian and dome-forming eruptions at Mt. Pelée volcano (Martinique, Lesser Antilles arc). J Volcanol Geotherm Res 96:191–206

Morton BR, Taylor GI, Turner JS (1956) Turbulent gravitational convection from maintained and instantaneous source. Proc R Soc Lond 234:1–23

Neri A, Di Muro A, Rosi M (2002) Mass partition during collapsing and transitionnal columns by using numerical simulations. J Volcanol Geotherm Res 115:1–18

Newhall CG, Self S (1982) The volcanic explosivity index (VEI): an estimate of explosive magnitude for historical volcanism. J Geophys Res 87:1231–1238

Pichavant M, Martel C, Bourdier JL, Scaillet B (2002) Physical conditions, structure, and dynamics of a zoned magma chamber: Mount Pelée (Martinique, Lesser Antilles Arc). J Geophys Res 107:315. doi:10.1029/2001JB000

Pyle DM (1989) The thickness, volume and grainsize of tephra fall deposits. Bull Volcanol 51:1–15

Pyle DM (1995) Mass and energy budgets of explosive volcanic eruptions. Geophys Res Lett 22:563–566

Roobol MJ, Smith AL (1976) Mount Pelée, Martinique: a pattern of alternating eruptive styles. Geology 4:521–524

Roobol MJ, Smith AL (1980) Pumice eruptions of the Lesser Antilles. Bull Volcanol 43:277–286

Ruzié L, Moreira M (2010) Magma degassing process during plinian eruptions. J Volcanol Geotherm Res 192:142–150

Sparks RSJ (1986) The dimensions and dynamics of volcanic eruption columns. Bull Volcanol 48:3–15

Traineau H (1982) Contribution à l'étude géologique de la Montagne Pelée (Martinique). Evolution de l'activité éruptive au cours de la période récente. PhD thesis, Université Paris XI

Traineau H, Westercamp D (1985) Les éruptions ponceuses récentes de la Montagne Pelée (Martinique). Description des dépôts-dynamique éruptifs. IMRG AFMM85 SGN 471:1–68

Traineau H, Westercamp D, Bardintzeff JM, Miskovsky JC (1989) The recent pumice eruptions of Mt. Pelée volcano, Martinique. Part I: Depositional sequences, description of pumiceous deposits. J Volcanol Geotherm Res 38:17–33

Villemant B, Boudon G (1998) Transition from dome-forming to plinian eruptive styles controlled by H_20 and Cl degassing. Nature 392:65–69

Villemant B, Boudon G (1999) H_20 and halogen (F, Cl, Br) behaviour during shallow magma degassing processes. Earth Planet Sci Lett 168:271–286

Villemant B, Boudon G, Komorowski JC (1996) U-series disequilibrium in arc magmas induced by water-magma interaction. Earth Planet Sci Lett 140:259–267

Walker GPL (1980) The Taupo pumice: product of the most powerful known (ultraplinian) eruption? J Volcanol Geotherm Res 8:69–94

Westercamp D, Traineau H (1983a) The past 5,000 years of volcanic activity at Mt. Pelée Martinique (F.W.I.): implications for assessment of volcanic hazards. J Volcanol Geotherm Res 17:159–185

Westercamp D, Traineau H (1983b) Carte Géologique au 1/20,000 de la Montagne Pelée. BRGM

Wilson L, Sparks RSJ, Walker GPL (1980) Explosive volcanic eruptions-IV. The control of magma properties and conduit geometry on eruption column behaviour. Geophys J R Astrom Soc 63:117–148

Woods AW (1988) The fluid dynamics and thermodynamics of eruption columns. Bull Volcanol 50:169–193

Woods AW, Bower SM (1995) The decompression of volcanic jets in a crater during explosive volcanic eruptions. Earth Planet Sci Lett 131:189–205